Multiparticle production in proton-nucleus collisions at 200 GeV

A. Klar and J. Hüfner

Institut für Theoretische Physik der Universität Heidelberg, Heidelberg, Federal Republic of Germany
and Max-Planck-Institut für Kernphysik, Heidelberg, Federal Republic of Germany
(Received 9 April 1984)

Rapidity distributions are analyzed for pp, pAr, and pXe collisions from a streamer-chamber experiment at 200 GeV. The distribution of negative particles is decomposed into a projectilelike and a targetlike component. In the distribution of the excess charge (positive minus negative particles) protons are separated from mesons. The analysis is somewhat model dependent. The shape of the various contributions, their integrated multiplicity, and their energy content are studied as a function of v, the number of struck nucleons. We calculate rapidity distributions using the fireball and multichain models, and compare them with the data.

I. INTRODUCTION

A proton of very high energy enters a nucleus, interacts with a row of target nucleons, is excited and excites the collision partners. After some time the excited baryons decay and a multiparticle final state is reached. Little is known about the space-time evolution of the process, although many experiments have been performed and several models proposed (cf., for example, Ref. 1). Two classes of experiments can be distinguished.

(i) One-particle inclusive measurements. Out of the many particles which are produced in each event, only one particle is observed, often in a magnetic spectrometer. The results are given in the form of an invariant cross section $E\,d^3\sigma/dp^3$.

(ii) Multiparticle measurements. All charged particles of an event are recorded. The devices are emulsions, bubble or streamer chambers, or other detectors with acceptance over a solid angle close to 4π. Observables are the distributions in multiplicity and in rapidity or various correlation functions.

Lately the results of a streamer-chamber experiment[2-4] have been published. We consider this experiment an important step forward over previous ones because a magnetic field is used. It permits us to separate positive from negative particles. We shall show that rapidity distributions of negative particles are much "cleaner" because they are not contaminated by protons. Because of the magnetic field the tracks in the streamer chamber are bent and the momentum of each particle is measured. (In most previous experiments only angles are determined.) With the new information the *energy* content of the particle production can be studied. Furthermore, events in the experiments[2-4] have also been classified by the number of "grey particles" (here protons with momenta p between 200 and 600 MeV/c), which permit a selection of the impact parameter in pA collisions and therefore measure the number v of struck nucleons.[5] The only drawback of the experiment lies in the fact that the mass of the particles has not been identified except for momenta $p < 600$ MeV/c. We consider this experiment an important step forward and therefore attempt a careful and detailed

analysis. In this way we hope to contribute to a deeper understanding of multiparticle production in hadron-nucleus collisions.

At present there are several models which are able to describe the available data.[6] They may be classified into more global approaches (e.g., coherent tube[7] or hydrodynamics[8]) or more microscopic ones (e.g., partons[9] or wounded quarks[10]). In our opinion the multichain model by Capella and Tran Thanh Van[11] has been the most detailed and most successful one lately. It relates the rapidity distribution of produced particles to the x distribution of quarks in the nucleons and to phenomenological fragmentation functions. No free parameter enters.

In this paper we decompose the experimental[2] rapidity distributions of the negative and positive particles into several contributions and study their variation with the number v of struck nucleons. We start with the proton-proton (pp) data (Sec. II), then proceed to the pAr and pXe data (Sec. III), and finally calculate particle distributions within the fireball model and the multichain approach (Sec. IV). We close with a summary and a conclusion (Sec. V).

II. RAPIDITY DISTRIBUTIONS FOR pp COLLISIONS

In the paper by De Marzo *et al.*,[2] rapidity distributions are published for negative and positive particles separately. We denote them by dn_-/dy and dn_+/dy, respectively. For pp collisions these distributions should be symmetric around the c.m. rapidity $y_{c.m.}$ ($y_{c.m.} = 3$ for 200 GeV). For the negative-particle distribution dn_-/dy, this symmetry is indeed observed within the experimental uncertainties. The distribution dn_+/dy of positive particles is manifestly asymmetric around $y_{c.m.}$. Why? In the experiment only the momentum of the particle has been measured by the curvature of the track, but the mass has not been identified except for very slow particles ($p < 600$ MeV/c). However, the rapidity of a particle with momentum $p = (p_{||},\mathbf{p}_\perp)$ is defined by

$$y = \ln\frac{p_{||}+(p_{||}^2+m_\perp^2)^{1/2}}{m_\perp} \qquad (1)$$
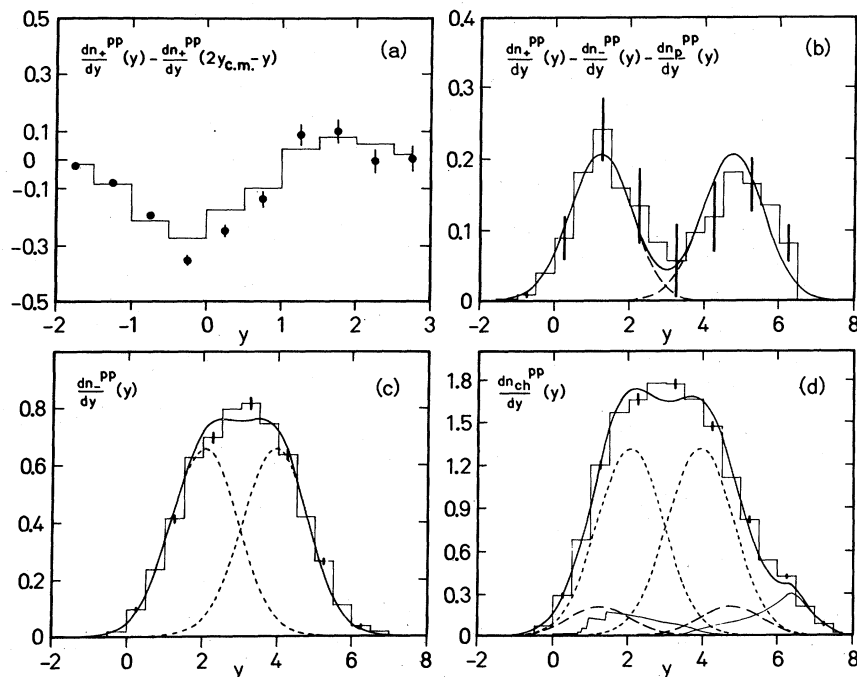
FIG. 1. Analysis of the rapidity distributions of charged particles in pp collisions. (a) The asymmetry of the positive particle distribution around the c.m. rapidity $y_{c.m.}$, Eq. (3). The points with error bars are calculated from the data. The histogram represents our best one-parameter fit, the shape being given in Eq. (5). (b) The distribution of excess charge. The histogram is calculated from the data. The solid curve is a fit assuming two Gaussians (broken lines) symmetric with respect to $y_{c.m.}$. (c) Distribution of negative particles. The dashed curves represent the targetlike and projectilelike Gaussians. The solid curve is their fitted sum. (d) The distribution of all charged particles. The curves represent the various contributions: protons (thin curve), leading and trailing pions (dashed curve), central pions (dotted curve). The solid curve is the sum of all contributions.

with the "transverse mass" $m_\perp^2 = m^2 + p_\perp^2$. Since in the experiment only p has been measured a value of rapidity has been assigned to each particle by *assuming* it to be a pion. This is certainly true for most particles, but there are also protons, kaons, and antiprotons among the particles. These are then misidentified. This misidentification produces the asymmetry in the rapidity distribution: the rapidity difference Δy between rapidities which are calculated with different masses μ and M ($\mu < M$) but with the momentum p is

$$\Delta y = y_\mu - y_M = \begin{cases} \ln M_\perp / \mu_\perp & \text{if } p_{||} \gg M_\perp \\ p_{||}(M_\perp - \mu_\perp)/M_\perp \mu_\perp & \text{if } p_{||} \ll \mu_\perp . \end{cases} \quad (2)$$

The rapidity shift is therefore different for small and large momenta, hence the asymmetry. For a proton misidentified as a pion $\ln(M_\perp / \mu_\perp) \simeq 1$, for a kaon misidentified as a pion $\ln(M_\perp / \mu_\perp) \approx 0.5$. The misidentification of kaons should show up as asymmetry in the negative particles, but is not seen. The reason might be their relatively small number of K^- (less than 10%) of all negatives, and the experimental rapidity bin size, which also equals 0.5. Antiprotons contribute of the order of 1% and can safely be neglected.

The asymmetry in dn_+/dy must be due to protons mostly (we exclude K^+, because K^- are not seen in the negatives). We turn the deficiency of the data into a virtue and use the asymmetry to separate protons from posi-

tive mesons. The experimental asymmetry

$$\frac{dn^{(\text{asy})}}{dy} = \frac{dn_+^{pp}}{dy}(y) - \frac{dn_+^{pp}}{dy}(2y_{c.m.} - y) \quad (3)$$

is shown as the points with error bars in Fig. 1(a). In order to extract the true rapidity distribution $dn^{pp \to pX}/dy$ from the observed asymmetry, we parametrize this function in a convenient way, "misidentify" the distribution and fit to the experimental quantity, Eq. (3). We choose

$$\frac{dn^{pp \to pX}}{dy} = a \left[\cosh(y - y_{c.m.}) + b \right] \quad 0 < y < 2y_{c.m.} \quad (4)$$

and for the total invariant cross section

$$E \frac{d^3\sigma}{dp^3} = \sigma_{\text{in}}^{pp} \frac{dn^{pp \to pX}}{dy} \frac{\alpha}{\pi} e^{-\alpha p_\perp^2} , \quad (5)$$

where α has been fixed to 4 GeV^{-2} and the total inelastic pp cross section σ_{in}^{pp} has been taken to be 30 mb. A parametrization like Eq. (4) is suggested by inclusive measurements[12] for $pp \to pX$ in which one finds $d\sigma/dx = \text{const}$, where x is the c.m. momentum fraction $x = p_{||}/p_0$. Transforming x into rapidity y leads to the dependence on the hyperbolic cosine [Eq. (4)]. Because of possible deviations from the hyperbolic-cosine law in the region of $y \approx y_{c.m.}$, we find it convenient to add a constant b to fit the experiment. Furthermore, we use the experimental information[12] for the total number of protons after

TABLE I. Summary of the analysis for the rapidity distributions of the pp data. Functional dependences, parameter values from best fits to the data, particle content $\langle n \rangle$, and integrated energy $\langle E \rangle$ are given for each contribution.

Contribution	Functional dependence	Fit parameters			$\langle n \rangle$	$\langle E \rangle$ (GeV)
		a	b			
Proton	$\dfrac{dn^{pp \to p,n}}{dy} = a\,[\cosh(y - y_{\text{c.m.}}) + b]$	0.048	0.51		1.1	58
Neutron		0.039	0.51		0.9	47
		A	σ	s_1		
Leading π^+	$\dfrac{dn^{pp \to \pi X}}{dy} = A\left[\exp\left(-\dfrac{(y - s_1)^2}{2\sigma^2}\right)\right.$	0.21	0.84	1.23	0.9	15
All π	$\left. + \exp\left(-\dfrac{[y - (2y_{\text{c.m.}} - s_1)]^2}{2\sigma^2}\right)\right]$	1.97	0.89	2.06	8.8	75
						$\sum = 195$

pp collisions to fix the integral of Eq. (4) to a value of 1.1. Roughly one baryon appears as a proton, the other as a neutron. Then Eq. (4) contains one degree of freedom. A fit to the experimental asymmetry leads to the values

$$a = 0.048, \quad b = 0.51 . \tag{6}$$

The extra incident charge $\Delta q = 2 - 1.1$ has been transferred to a positive pion. In order to locate the excess charge in rapidity we define its distribution by

$$\frac{dn^{(\text{EC})}}{dy} = \frac{dn^{pp}_+}{dy} - \frac{dn^{pp}_-}{dy} - \frac{dn^{pp}}{dy} . \tag{7}$$

The histogram in Fig. 1(b) shows the result: two well-separated peaks appear at $y = 1.2$ and $y = 4.8$. We fit these by Gaussians, which are also shown and the parameters of which are found in Table I.

In the last step we analyze the rapidity distribution of the negative particles. Because of the symmetry already observed, we fit them by two Gaussians, which are situated symmetrically around $y_{\text{c.m.}}$. Why two functions and why Gaussians? No deep justification can be given for the Gaussian shape, except that it is convenient and yields a good fit. The decomposition of the negative particles into *two* components is supported by an experimental and a theoretical observation:

(a) In pA collisions dn^{pA}_- / dy does not increase homogeneously over the full rapidity interval as A increases, but mostly in the range $y \lesssim y_{\text{c.m.}}$, i.e., in the targetlike region, while the projectile region remains essentially unaffected. This observation leads to postulate a targetlike and a projectilelike component.

(b) The multichain model[11] for pp collisions predicts the dominant contribution for multiparticle production to arise from two "chains." One leads to fast produced particles, the other to slow ones.

The result of fitting dn_- / dy by two Gaussians is shown in Fig. 1(c) and the parameters are listed in Table I.

Energies are calculated for each component by using

$$\langle E \rangle = \int dy \langle m_\perp \rangle \cosh(y) \frac{dn}{dy} , \tag{8}$$

where $\langle m^\pi_\perp \rangle = 0.39$ GeV and $\langle m^p_\perp \rangle = 1.05$ GeV are the transverse masses of the pion and the proton, respectively. Values for $\langle E \rangle$ are listed in Table I. Figure 1(d) shows the total charged-particle spectrum together with the decomposition into the various components and contributions. They are the following.

(i) The baryons. If one neglects $N\bar{N}$ production, two baryons are expected in the final state, about one of them appears as a proton (the other is a neutron and is not seen). The total energy carried by the baryons is 50% of the incident energy. Their distribution is given by the two nonsymmetric curves of Fig. 1(d).

(ii) The leading mesons which carry the excess charge. On the average there is one meson, which carries the excess charge. This particle has a significant fraction (7.5%) of the incident energy. Its distribution is given by the two smaller symmetric Gaussians of Fig. 1(d).

(iii) The bulk of the produced particles. We define them as three times the negative particles. Their total multiplicity amounts to nine particles and they carry about 40% of the incident energy. Their distribution is shown as the two larger symmetric Gaussians in Fig. 1(d).

We note that the energy contained in the three contributions adds up to 195 GeV, which coincides with the projectile energy within the uncertainty of the analysis.

III. MULTIPARTICLE PRODUCTION IN PROTON-NUCLEUS COLLISIONS

In the pA collisions two additional complications arise as compared to the pp case.

(a) The results are not expected to be symmetric around $y_{\text{c.m.}}$, neither for the negative nor for the positive particles. Thus protons cannot be separated from mesons as was possible for the pp data.

(b) Because of the intranuclear cascade inside the nucleus, we expect quite a number of protons to show up in the rapidity distribution of positive particles, especially in the targetlike region. As shown below this is also the place where most of the nuclear effect for the multiparticle *production* appears.

For the above reasons the rapidity distribution of posi-

TABLE II. Particle and energy content of the difference function $D(y,\nu)$ as a function of ν, the number of struck nucleons. We give the mean number $\langle n_-\rangle_\nu$ and the mean energy $\langle E_-\rangle_\nu$ in $D(y,\nu)$, Eq. (14) for each ν; $D(y,\nu)$ has been fitted to a Gaussian, the width σ and position s of which are given in the last two rows.

ν	2.2	2.25	2.7	3.25	3.6	4.4	5.0
$\langle n_-\rangle_\nu - \langle n_-\rangle_{pp}$	2.06±0.15	2.40±0.12	2.79±0.20	3.85±0.08	4.44±0.29	5.66±0.34	6.57±0.45
$\langle E_-\rangle_\nu - \langle E_-\rangle_{pp}$	8.32±1.17	8.25±0.90	8.81±1.48	11.67±0.57	14.97±2.11	13.77±2.02	17.16±2.64
σ	1.25	1.33	1.31	1.33	1.40	1.28	1.38
s	2.32	2.05	2.04	1.93	1.90	1.77	1.76

tive particles is essentially useless for the study of the multiparticle *production* phenomena in pA collisions. Thus we study the rapidity distribution of negative particles dn_-/dy.

In earlier times one has often studied the *ratio* of pA to pp distributions:

$$R(y) = \frac{dn_-^{pA}}{dy} \Big/ \frac{dn_-^{pp}}{dy} . \qquad (9)$$

We find it more instructive to study the *difference*:

$$D(y,\nu) = \frac{dn_-^{pA}}{dy}(y,\nu) - \frac{dn_-^{pp}}{dy}(y) . \qquad (10)$$

Here the variable ν denotes the number of struck nucleons. This number can be controlled in two ways. First, if one uses all events with a fixed target nucleus A, then ν has to be identified with the average value

$$\bar\nu = \frac{A\sigma_{\text{in}}^{pp}}{\sigma_{\text{in}}^{pA}} , \qquad (11)$$

where the inelastic reaction cross section σ_{in}^{pA} is calculated with the inelastic pp cross section

$$\sigma_{\text{in}}^{pA} = \int d^2b \left[1 - \exp\left[-\sigma_{\text{in}}^{pp} \int dz\, \rho_A(b,z) \right] \right] . \qquad (12)$$

The definition Eq. (11) slightly differs from the one commonly used by the appearance of σ_{in}^{pA} instead of the experimental reaction cross section. We think Eq. (11) is more appropriate since ν denotes really the number of inelastic collisions in the target. We have

$$\bar\nu = 2.25, \; p\text{Ar}, \quad \bar\nu = 3.25, \; p\text{Xe} . \qquad (13)$$

The second way to control ν is by selecting events with a fixed number of "grey" particles n_p. In our analysis both methods are employed.

Figure 2 shows the difference function $D(y,\nu)$, Eq. (10), for a few selected values of ν. It is mainly located in the targetlike side of the rapidity interval ($y < y_{\text{c.m.}}$). It grows with ν and the shape does not change significantly. For the values of ν shown in the figure and some additional values we have determined the particle and the energy content of $D(y,\nu)$

$$\langle n_-\rangle_\nu - \langle n_-\rangle_{pp} = \int dy\, D(y,\nu) ,$$

$$\langle E_-\rangle_\nu - \langle E_-\rangle_{pp} = \int dy\, \langle m_\perp^\pi \rangle \cosh(y) D(y,\nu) . \qquad (14)$$

These numbers are shown in Table II. In order to determine the total energy which goes into particle production

as a function of ν we take three times the values of Table II, allowing for the three charge states of the pion. (As will be argued below the contribution of leading pions does not change from pp to pA collisions.)

The mean number of particles $\langle n_-\rangle_\nu$ is strictly proportional to ν up to the highest observed value $\nu = 5$, cf. Fig. 3:

$$\langle n_-\rangle_\nu = \langle n_-\rangle_{pp}[1 + \beta(\nu - 1)] . \qquad (15)$$

This relation has mostly been observed for all charged particles in earlier work. However, the positive particles are contaminated by protons which may explain the uncertainties in the value of $\beta = 0.5 \pm 0.2$ (cf. Ref. 6). In Fig. 3 the relation is confirmed for negative particles and we find

$$\beta = 0.57 \pm 0.04 . \qquad (16)$$

The energy content in the spectra grows, however, more slowly than $(\nu - 1)$. This is shown in Fig. 3, where the points clearly deviate from a horizontal line. Furthermore, going from the first to the second collision much less energy is lost into particle production than in the first collision.
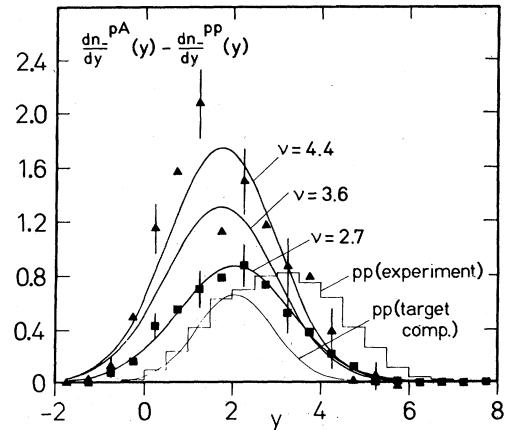
FIG. 2. The difference $D(y,\nu)$ in the distribution of the negative particles for pA and pp collisions. The points give experimental values of D for two values of ν ($\nu = 2.7$: squares, $\nu = 4.4$: triangles). The solid curves represent the best-fit Gaussians to the data at $\nu = 2.7$, 3.6, and 4.4. For comparison we show the experimental distribution of negative particles from pp collisions and the targetlike component in this pp distribution [from Fig. 1(c)].
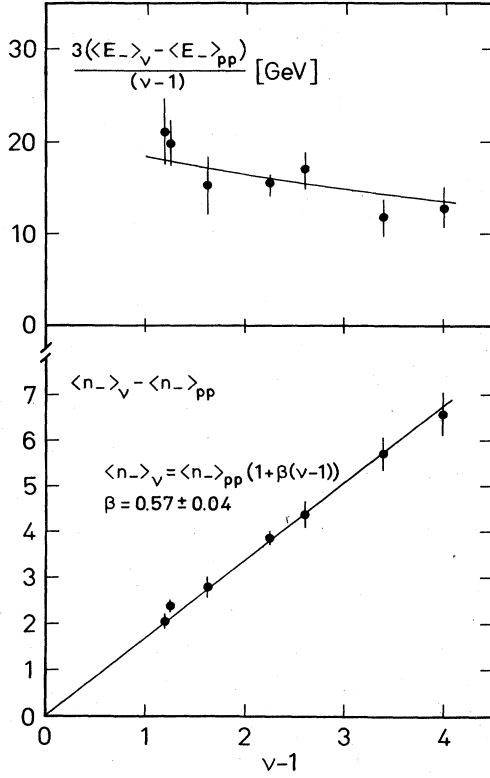
FIG. 3. The experimental mean number of particles ($\langle n_- \rangle_v - \langle n_- \rangle_{pp}$) (lower graph) and the energy content $3(\langle E_- \rangle_v - \langle E_- \rangle_{pp})$ (upper graph) in $D(y,v)$ as a function of $v-1$. Note that the energy content has been divided by $(v-1)$ in order to show that the energy grows more slowly than $(v-1)$. The straight line in the lower graph is a best fit to the data. The solid curve above is calculated using Eq. (20).

In a simple model[13] for the nuclear stopping power we have derived a relation for the asymptotic mean energies of the nucleon after v inelastic collisions:

$$\langle E_p \rangle_v = (1-I)^{v-1} \langle E_p \rangle_{pp} ,\qquad (18)$$

where $I \approx 0.2$. Since the energy lost by the proton must appear as the energy of produced mesons, we have the relation

$$3[\langle E_- \rangle_v - \langle E_- \rangle_{pp}] = \langle E_p \rangle_{pp} - \langle E_p \rangle_v ,\qquad (19)$$

where the factor 3 accounts for the three charge states of the pion. Using Eq. (18)

$$3[\langle E_- \rangle_v - \langle E_- \rangle_{pp}] = [1 - (1-I)^{v-1}]\langle E_- \rangle_{pp} .\qquad (20)$$

The solid line in Fig. 3 shows the dependence on v as predicted by Eq. (20) where we use $I=0.18$ (Ref. 13). It remains unclear to us why the *number* $\langle n_- \rangle_v$ of produced particles strictly increases with v, while the *energy* content in the produced particles $\langle E_- \rangle_v$ grows more slowly.

We come back to the fact that the number of negative particles is strictly proportional to v and no quadratic terms are found. We take this as one evidence for the absence of cascading of the *mesons*. It has been observed

previously that the ratio $R(y,v)$, Eq. (9), for *all* charged particles rises with v more rapidly than linearly for small rapidities ($y \lesssim 1$). This has been interpreted as an effect of cascading: mesons with small rapidities reach their asymptotic state *inside* the nucleus, rescatter, and produce new particles. Part of the effect, which has been observed earlier, is certainly due to the proton contamination and was not interpreted correctly. But we also seen an effect in the negative particles: for small values of y the number of π^- rises more rapidly than v. From our analysis we conclude that this is not an effect of cascading but rather of the fact that the proton loses less and less energy, Eq. (18). We explain our argument: if we fit the difference function $D(y,v)$ by one Gaussian, the *width* of this Gaussian is independent of σ, thus there is no broadening (no cascading) (see Table II). The *particle content of* the Gaussian rises strictly proportionally to $v-1$ (no particle production). The *position*, however, shifts downward in rapidity, thus making the energy smaller. This shift is the origin of the nonlinear behavior of $R(y,v)$ for small y.

We turn to the rapidity distribution of the positive particles. It contains the leading proton (mostly at $y > y_{\text{c.m.}}$), leading mesons which carry the charge excess (also at $y > y_{\text{c.m.}}$), target protons (mostly at $y < y_{\text{c.m.}}$), and the bulk positive mesons (distributed over the full rapidity interval). By definition the distribution of the bulk positive mesons is identical with the one of the negative mesons. Since the distribution of the negative mesons has been studied, we concentrate here on the remainder

$$\frac{dn^{(\text{CE})}}{dy} = \frac{dn_+^{pA}}{dy} - \frac{dn_-^{pA}}{dy} .\qquad (21)$$

The histogram for this distribution is shown in Fig. 4 for the pAr and pXe collisions. The large peak for $y < y_{\text{c.m.}}$ mostly consists of target nucleons (including cascade ones). We do not attempt to describe them. The projectilelike side ($y > y_{\text{c.m.}}$) contains the leading proton and the mesons, which carry the excess charge. In order to describe the experimental distribution we calculate the distribution of the protons within the approach by Hüfner and Klar[13] and assume the distribution of the excess charge pions in pA collisions to be the same as that for pp collisions. This assumption is supported by the A dependence of the inclusive cross section for $pA \rightarrow \pi^+ X$ (Barton *et al.*[14]). The lines in Fig. 4 show the results of our approach. Within the error bars $dn^{(\text{CE})}/dy$ can be quantitatively described by the π^+ carrying the excess charge and by the protons. However, it remains a puzzle to us why the π^+ distribution is independent of A, while the distribution of the leading protons changes dramatically with A.

IV. CALCULATION OF RAPIDITY DISTRIBUTIONS WITHIN THE FIREBALL AND THE MULTICHAIN MODELS

As mentioned in the Introduction several models explain the gross features of multiparticle production in nuclei. In this work we are able to study the production phenomena more thoroughly by analyzing the rapidity distribution of the negative particles. Here we want to
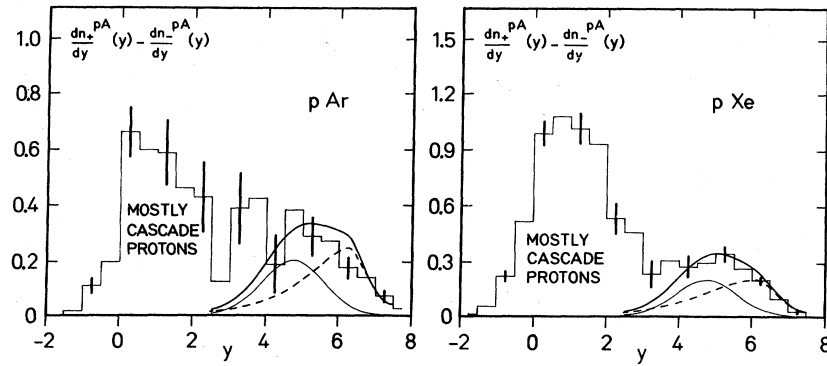
FIG. 4. The distribution of the excess charge in pAr (left) and pXe (right) collisions. The histogram represents the data. The dashed curve describes the leading proton and the thin curve the leading pions. The solid curve is their sum.

calculate the spectra of produced particles using two complementary models: The *fireball model* is a global model based on energy conservation and the assumption of thermalization. The *multichain model* is a microscopic model, which assumes a detailed mechanism for the production and uses quark distributions and fragmentation functions from other experiments as input (Fig. 5).

First of all we treat the two-fireball model for pp collisions (it closely resembles the model by Jacob and Slansky[15]): two protons collide, part of their kinetic energy is converted into excitation energy. The excited nucleons come to thermal equilibrium ("fireballs") and decay according to the laws of thermodynamics. In the following all quantities refer to the c.m. system. If the protons have initial rapidities $\pm y_0$, rapidities of the fireballs are $\pm y$. Since a nucleon is much heavier than a pion, we assume the fireball rapidity to be the same as that of the finally observed nucleon. This assumption is very convenient, because the rapidity distributions $dn^{pp \to pX}/dy$ of the final protons are known experimentally, Eq. (4). The excitation energy $E^*(y)$ of the fireball is calculated from the energy difference between the initial and the final states of the proton:

$$E^*(y) = M \cosh(y_0) - M_\perp \cosh(y) , \qquad (22)$$
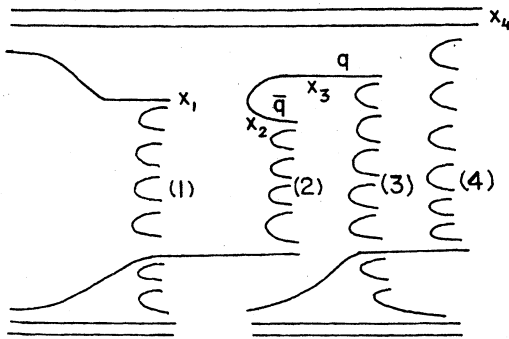
FIG. 5. Representation of chains 1—4 in the multichain model; the figure is taken from Ref. 11. The upper lines represent the quarks of the projectile nucleon, while several target nucleons are displayed at the lower side.

where M is the rest mass and $M_\perp$ is the transverse mass of a proton. The fireball decays in its rest system into $n_\pi(y)$ pions. Their momentum distribution is governed by the temperature T. Its value $T = 110$ MeV is so determined as to give the experimentally observed mean transverse momentum of the pions. Therefore T is not the temperature of the fireball but rather the "freeze-out" temperature. The momentum distribution of the pions from the decay of the fireball is therefore

$$E \frac{d^3 W}{dp^3} = C(T) \frac{E(p)}{e^{E/T} - 1} n_\pi(y) , \qquad (23)$$

where p is measured in the rest system of the fireball and $C(T)$ is a normalization constant,

$$\int d^3 p \frac{C(T)}{e^{E/T} - 1} = 1 .$$

The number $n_\pi(y)$ of produced pions is fixed by requiring that the energy contained in Eq. (23) equals the excitation energy given by Eq. (22). The final distribution of pions is then the result of a superposition of fireball distributions where the weight is given by the empirically determined distribution of nucleons, Eq. (4):

$$\frac{dn^{pp \to \pi X}}{dy} = \int dy' \frac{dn^{pp \to pX}}{dy'} \int d^2 p_\perp E \frac{d^3 W}{dp^3} (\mathbf{p}_\perp, y - y') . \qquad (24)$$

Figure 6(a) shows the result of such a parameter-free calculation compared with the data. The shape and absolute magnitude of the data are well reproduced. However, for pion production in proton-nucleus collisions, the above model fails to describe the data. The calculated number of particles in the projectilelike region is about twice as large as the observed one. The reason is the following: from the analysis of the difference function $D(y, v)$ we have learned: after the first collision the projectile nucleon mainly loses energy by exciting target nucleons and not by being itself further excited. We have not been able to devise a simple model which includes this physics and which conserves energy and momentum.

The basic idea of the approach of Capella and Tran Thanh Van[11] is depicted in Fig. 5. A proton represented
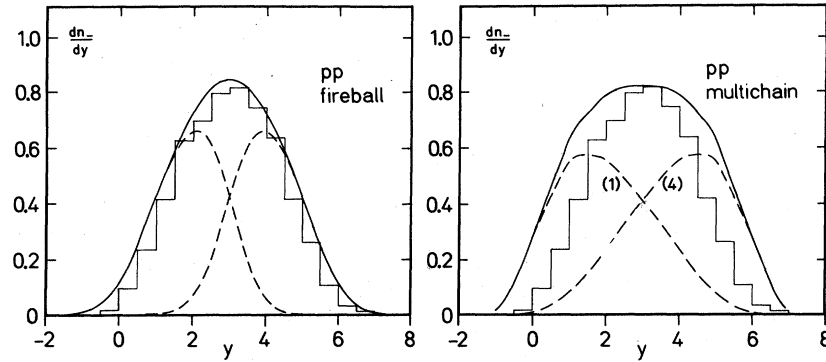
FIG. 6. Calculation of negative particle distributions for pp collisions. Left: fireball model. The dashed curves represent the contributions from the target and projectilelike fireballs, respectively. The solid curve is their sum. Right: same picture showing the calculation with two-chain model, Ref. 11. The numbers refer to the chains and are explained in the text.

by the three valence quarks interacts with a target nucleon; after the interaction the nucleons separate into a quark and a diquark, which carry color. A color string forms between corresponding objects from the target and the projectile nucleons. The strings are called "chains" and they are the sources of meson production. Chain 1 forms between the projectile quark with momentum fraction x and the diquark of the target nucleon. In subsequent interactions with the target nucleons the remaining projectile diquark remains inert and chains are formed only with the sea quarks of the projectile. These chains are denoted by chain 2 and chain 3. Finally there is one chain (called chain 4) between the last target nucleon and the projectile. For pp collisions only chains 1 and 4 appear. The pion distribution is then a superposition of events with different numbers v of target nucleons:

$$\frac{dn^{pA \to \pi X}}{dy}(y) = \sum_{v \geq 1} W_v \{ N_1^\pi(y,v) + N_4^\pi(y,v) + (v-1)[N_2^\pi(y,v) + N_3^\pi(y,v)] \} \ . \tag{25}$$

Here W_v denotes the probability for v-fold scattering of the projectile in the nucleus, the N_a ($a = 1-4$) are the contributions of the various chains, which are formed between valence quarks, sea quarks, and diquarks as depicted in Fig. 5. As an example we give the formula for $N_1(y)$. Chain 1 stretches between a quark of the projectile and the diquark of the first struck target nucleon. The distributions of their respective momentum fractions x are denoted by $\rho_v(x,x')$ and are calculated from the quark distribution functions taking momentum conservation on the quark level into account. The explicit structure is given by

$$N_1^\pi(y,v) = \int_0^1 dx \, dx' \rho_v(x,x') F_{q,qq}(y;x,x') \ . \tag{26}$$

Here $F_{q,qq}$ is the fragmentation function for a chain stretched between a quark at x and a diquark at x'. This function is taken from hadronization phenomena in e^+e^- and e^-p collisions. The functions F depend on the values x and x' at their boundaries. Using Eqs. (25) and (26) we have calculated pion distributions for pp as well as for pA collisions. The result for the dn_-/dy is shown in Fig. 6(b), those for the pp collision and for the pAr and pXe experiments in Fig. 7. We also display the contributions from the various chains.

We discuss the pp results first. The multichain model clearly has a two-component structure for the pion distribution. Chain 1 is located in the targetlike region, while chain 4 is located in the projectilelike one. The shape of each is asymmetric and does not look like a Gaussian. This is in contrast to our assumption [Fig. 1(d)] and also to the fireball model. The multichain model, with parameters taken from Ref. 11, gives too broad a distribution for the π^- and thus predicts too much energy in the meson production. This fact is most easily seen in the spectra of the negative particles. Usually one compares the distribution of all produced particles with the calculation. Then the agreement seems better, however, for the wrong reasons. Misidentified protons significantly contribute to widen the experimental distribution and let the discrepancies in the projectilelike region nearly disappear. Obviously, energy conservation is not taken into account properly, because all the calculated spectra contain more energy than the experimental ones. This is not a defect of the multichain model but of the particular parametrization for the fragmentation function (cf. Ref. 16 for other parametrizations). The results for the pA calculation are given in Fig. 7. In this case, too, the two-component structure is evident. Only one chain—chain 4—is connected to the projectile diquark and populates the projectilelike region. In the targetlike region $y < y_{c.m.}$ chains 1 and 3 contribute, while chain 2 is rather unimportant. The increase in pion multiplicity with $v - 1$ is mostly due
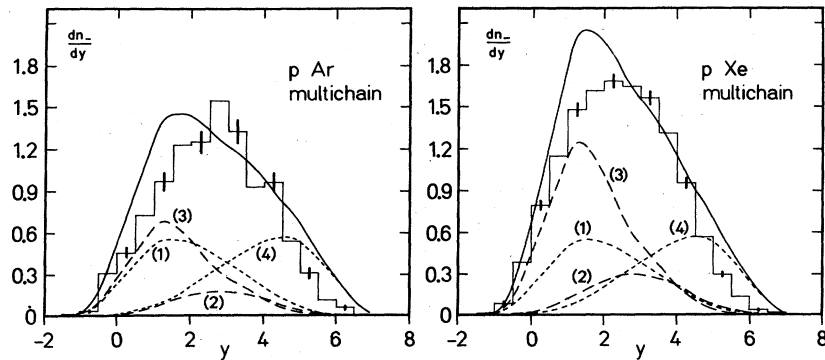
FIG. 7. Calculation of spectra for negative particles for pAr and pXe collisions in the multichain model. The dotted curves represent the contributions of chains 1 and 4 of the model of Ref. 11. The dashed curves refer to chains 2 and 3 and are the contributions from multiple scattering. The solid curve is the sum of the four.

to chain 3. The calculations agree in an overall way with the data.

V. CONCLUSION

We have analyzed rapidity distributions for charged particles observed in a streamer-chamber experiment with magnetic field. The experimental distributions have been decomposed into several contributions, protons, leading pions, and central or bulk pions. We have found the distributions of the negative particles most instructive, since they are free of protons and leading pions and thus display most cleanly the features of multiparticle production in proton-nucleus collisions. The distribution of negative particles shows two components, one located in the projectilelike region, the other in the targetlike region. In

pA collisions only the component on the target side in rapidity space grows with v. The number of produced particles grows strictly linearly with v, while their energy content rises more slowly. We cannot see any effect of cascading for the mesons at small rapidity. The basic features of the empirical data can be reproduced in calculations based on the multichain model.

[1]*Proceedings of the First Workshop on Ultrarelativistic Nuclear Collisions, Berkeley, California, 1979* (Report No. LBL-8957, 1979); I. Otterlund, in *Quark Matter '83,* proceedings of the Third International Conference on Ultrarelativistic Nucleus-Nucleus Collisions, Brookhaven National Laboratory, 1983, edited by T. W. Ludlam and H. E. Wegner [Nucl. Phys. A418, 87c (1984)].

[2]C. De Marzo et al., Phys. Rev. D 26, 1019 (1982); and I. Derado (private communication).

[3]C. De Marzo et al., Phys. Rev. D 29, 2476 (1984).

[4]C. De Marzo et al., Phys. Rev. D 29, 363 (1984).

[5]J. Babecki and G. Novak, Acta Phys. Pol. B 9, 401 (1978); E. Stenlund and I. Otterlund, Nucl. Phys. B198, 407 (1982); M. K. Hegab and J. Hüfner, Phys. Lett. 105B, 103 (1981); N. Suzuki, Nucl. Phys. A403, 553 (1983).

[6]W. Q. Chao, M. K. Hegab, and J. Hüfner, Nucl. Phys. A395,

482 (1983).

[7]G. Berlad, A. Dar, and G. Eilam, Phys. Rev. D 13, 161 (1976).

[8]K. Gottfried, Phys. Rev. Lett. 32, 957 (1974).

[9]S. J. Brodsky, J. F. Gunion, and H. J. Kühn, Phys. Rev. Lett. 39, 1120 (1977).

[10]N. N. Nikolaev and A. Ya. Ostapchuk, CERN Report No. TH 2575, 1978 (unpublished); A. Białas, W. Czyz, and W. Furmanski, Acta Phys. Pol. B 10, 831 (1979).

[11]A. Capella and J. Tran Thanh Van, Phys. Lett. 93B, 146 (1980); Z. Phys. C 10, 249 (1981).

[12]J. Whitmore, Phys. Rep. 10C, 273 (1974).

[13]J. Hüfner and A. Klar (unpublished).

[14]D. S. Barton et al., Phys. Rev. D 27, 2580 (1983).

[15]M. Jacob and R. Slansky, Phys. Rev. D 5, 1847 (1972).

[16]A. Capella, U. Sukhatme, and J. Tran Thanh Van, Phys. Lett. 119B, 220 (1962).